Growth kinetics of carbon nanowall-like structures in low-temperature plasmas

I. Levchenko, K. Ostrikov, A. E. Rider, E. Tam, S. V. Vladimirov, and S. Xu

Citation: Physics of Plasmas (1994-present) **14**, 063502 (2007); doi: 10.1063/1.2744353
View online: http://dx.doi.org/10.1063/1.2744353
View Table of Contents: http://scitation.aip.org/content/aip/journal/pop/14/6?ver=pdfcov
Published by the AIP Publishing

Growth kinetics of carbon nanowall-like structures in low-temperature plasmas

I. Levchenko, K. Ostrikov,[a] A. E. Rider, E. Tam, and S. V. Vladimirov
Plasma Nanoscience@Complex Systems, School of Physics, The University of Sydney, Sydney NSW 2006, Australia

S. Xu
Plasma Sources and Application Center, NIE, and Institute of Advanced Studies, Nanyang Technological University, 637616 Singapore

(Received 26 April 2007; accepted 8 May 2007; published online 19 June 2007)

The results of a hybrid numerical simulation of the growth kinetics of carbon nanowall-like nanostructures in the plasma and neutral gas synthesis processes are presented. The low-temperature plasma-based process was found to have a significant advantage over the purely neutral flux deposition in providing the uniform size distribution of the nanostructures. It is shown that the nanowall width uniformity is the best (square deviations not exceeding 1.05) in high-density plasmas of 3.0×10^{18} m^{-3}, worsens in lower-density plasmas (up to 1.5 in 1.0×10^{17} m^{-3} plasmas), and is the worst (up to 1.9) in the neutral gas-based process. This effect has been attributed to the focusing of ion fluxes by irregular electric field in the vicinity of plasma-grown nanostructures on substrate biased with −20 V potential, and differences in the two-dimensional adatom diffusion fluxes in the plasma and neutral gas-based processes. The results of our numerical simulations are consistent with the available experimental reports on the effect of the plasma process parameters on the sizes and shapes of relevant nanostructures. © *2007 American Institute of Physics*.
[DOI: 10.1063/1.2744353]

I. INTRODUCTION

Nanostructures of reduced dimensionality (one-dimensional and quasi-two-dimensional) have recently been of an enormous interest from the basic research and applications points of view. Nanoribbons for waveguide applications,[1] nanobelts for hydrogen storage, optical and microelectronics applications,[2] nanowalls,[3,4] nanorods for gas sensors,[5,6] nanocombs[7] and nanowires[8] for electronic and optoelectronic devices, and nanorings for magnetic data storage media[9] are just a few examples of the relevant nanostructures. Many unique properties of such nanostructures are determined by their geometrical parameters such as height, width, height-to-width ratio, and size distributions of all dimensions involved, which are determined in turn by the synthesis method used.[10] The range of dimensions of the quasi-two-dimensional nanostructures, which are in the spotlight of this work, is particularly wide spanning from ~10 nm widths to submicrometer heights and macroscopic (exceeding 1 mm) lengths.

The existing gas-based processes to synthesize such nanostructures can be split into two main categories, namely the neutral and plasma-based processes.[11,12] The plasma-enhanced chemical vapor deposition (PECVD) and plasma-aided treatment show significant advantages in the synthesis of various one-dimensional (1D) nanostructures, such as nanotubes and nanofibres, as compared with the processes based on the deposition of neutral flux to the wafer surface (e.g., CVD).[13,14] However, thermal chemical vapor deposition systems are in most cases simpler and consume less power. Therefore, the use of low-pressure plasma-based nanotools, which require additional power supplies, vacuum equipment, control and diagnostic instrumentation,[15] etc., needs to be well justified in terms of better performance in the fabrication of the nanostructures with the required properties, which is commonly referred to as the deterministic nanofabrication.[16]

Here we use a multiscale hybrid numerical simulation to demonstrate that the morphology of quasi-two-dimensional surface nanopatterns can be effectively controlled in an ionized gas-based process. We will show that using an ion flux extracted from the plasma makes it possible to control the shapes and sizes of the nanowalls better than in a neutral gas process. In particular, the size uniformity of such nanostructures appears much better in the plasma-based process.

This paper is organized as follows. In Sec. II, we present the model that was used in the numerical simulation of the development of the surface morphology in the neutral and ionized gas-based processes. This model involves a Monte Carlo (MC) simulation of ion deposition onto the nanostructured surface and a two-dimensional problem related to adatom diffusion on the surface. In Sec. III, the results of our numerical simulations are described. Finally, discussions in Sec. IV help one to interpret the numerical results and elucidate the physics behind the quite different growth of the quasi-two-dimensional nanopatterns in the neutral gas- and plasma-based nanofabrication processes.

[a]Author to whom correspondence should be addressed. k.ostrikov@physics.usyd.edu.au

II. MODEL AND NUMERICAL METHOD

In this work, we simulate the development of the surface nanopattern, which consists of the quasi-two-dimensional nanostructures (nanowalls) separated by trenches as shown in Fig. 1(a). In the neutral gas-based process, we assume that the neutral flux is uniformly deposited onto the surface. In the plasma process, the growth process is strongly affected by the ion fluxes extracted from the plasma and can be controlled by the plasma parameters and dc surface bias. The plasma is separated from the nanostructured surface by a presheath, a sheath, and a thin layer of nanostructured electric field [Fig. 1(b)]. In the presheath, the potential drop can be calculated,

$$U_P(z) = U_0[(z + \Delta_p)/\Delta_p]^2, \tag{1}$$

where U_0 is the potential at the sheath-presheath border [Fig. 1(b)], z is the distance to the presheath-sheath border [Fig. 1(b)], and Δ_p is the presheath width.[17,18] It is known that the total potential drop in the presheath has the order of $T_e/2$, where T_e is the electron temperature.[19] In the sheath, an uncompensated charge is present that produces a much stronger electric field, which can be obtained by solving the Poisson equation

$$\varepsilon_0 \Delta U = -e[\rho_i - \rho_e], \tag{2}$$

where ρ_i and ρ_e are the ion and electron densities, e is the electron charge, and ε_0 is the dielectric constant of the vacuum. It is known that the electrical field is mainly present in the sheath,[20,21] and it is low in the presheath area.[22]

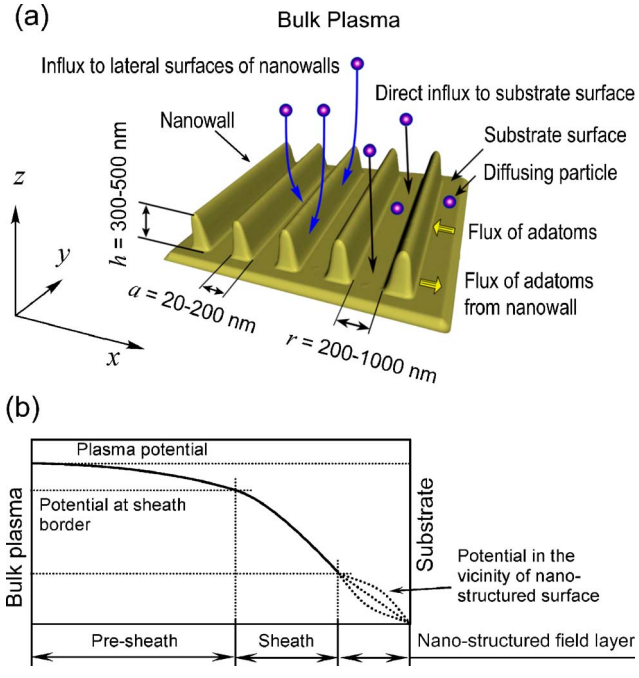

FIG. 1. (Color online) (a) Scheme of the system considered. Main dimensions of linear quasi-two-dimensional nanostructures (nanowalls) used in simulations, and schematic representation of interaction of neutral and charged particles with the nanostructured surface; (b) scheme of potential distribution in the whole system. In the simulation domain, the profile of the electric potential is a three-dimensional function dependent on nanowall shape (nanostructured field).

For simplicity, we do not specify the mechanism of the plasma generation and do not consider the processes in the plasma bulk, which can vary from one plasma source to another.[23] Instead, we consider the delivery of neutral and ionized carbon atoms from a low-temperature, weakly ionized plasma,[24] which can be generated in a range of plasma sources including nonequilibrium glow discharges, vacuum arcs, plasma-assisted sputtering, or hybrid facilities.[25–27] Thus, the ion flux is mainly accelerated in the sheath and is affected by the irregular electric field[28] created by the surface nanopattern. The ions are accelerated in the sheath (with the width λ_s) to the energy equal to the substrate bias U_S.

Some of the neutral/ionized atoms extracted from the plasma land in trenches between the nanowalls, while the others are deposited directly on the lateral surfaces of the nanostructures as shown in Fig. 1(a). The directly deposited particles (direct influx) are assumed to contribute to the nanostructure growth at the collision point. On the other hand, the particles arrived at open surface areas diffuse about the surface until they incorporate into the nearest nanowall. The model of the surface morphology formation from the ion and diffusion fluxes invokes an assumption that the energy of the ions deposited on the lateral surfaces of the quasi-two-dimensional structures is sufficient enough for activation of hydrogen-terminated surface bonds,[11] and thus an ion that hits the nanowall surface instantly incorporates into the reconstructed surface at the point of collision. To determine an ion current distribution on the substrate surface and lateral surfaces of the nanostructures, we implemented a Monte Carlo technique. The ion trajectory in the plasma-surface sheath was simulated by integrating the ion motion equations. The electric field was calculated as a sum of the regular field E_S produced by the biased open surface areas, and the irregular (microscopic) component E' produced by the quasi-two-dimensional nanostructures. Each ion trace was simulated separately using the total electric field E_S+E', and the information about hit point coordinates was accumulated in a data matrix. An initial position for each ion was set at the sheath border located at distance λ_s from the surface. The ion movement was simulated in the simulation domain limited by the substrate surface and the plasma sheath border. More specific details of the model of ion motion and numerical model can be found elsewhere.[29–31]

Two-dimensional flux of adatoms ψ_s to the nanostructure borders can be obtained by solving the diffusion equation

$$\frac{\partial \xi}{\partial t} = D_S\left(\frac{\partial^2 \xi}{\partial x^2} + \frac{\partial^2 \xi}{\partial y^2}\right) + \psi_{\text{ext}} - \psi_{\text{evp}} \tag{3}$$

for the adatom surface density $\xi(x,y,t)$, where ψ_{ext} is the external flux of particles to the substrate surface, $m^{-2}s^{-1}$; ψ_{evp} is the evaporation flux from the substrate surface, $m^{-2}s^{-1}$; and x, y are the Cartesian coordinates. The total surface flux, s^{-1}, of adsorbed species to the borders of nanostructure is then

$$\psi_S = -l\left[D_S\frac{\partial\xi}{\partial x}\right]_{x_B}, \tag{4}$$

where l is the perimeter of the nanowall, D_S is the surface diffusion coefficient, and x_B denotes the border location of the nanowalls with the longest dimension being in the y direction, as shown in Fig. 1(a). The surface diffusion coefficient is $D_S=\frac{\lambda^2}{4}\nu_0\exp(-\varepsilon_d/kT)$, where ε_d is the surface diffusion activation energy, λ is the lattice constant, ν_0 is the frequency of lattice atom oscillations, T is the surface temperature, and k is Boltzmann's constant. The total influx of atomic/ionic particles to the nanowall, s^{-1},

$$\psi_T(t) = \psi_D(t) + \psi_S(t) - \psi_{DE}(t) - \psi_{BE}(t), \tag{5}$$

where ψ_D is the flux of particles directly to the nanostructure surface, which is calculated by invoking the ion motion model described above, ψ_{DE} is the evaporation flux from the nanostructure surface to the gas/plasma bulk $\psi_{DE}=\frac{S}{\lambda^2}\nu_0\exp(-\varepsilon_a/kT)$, where S is the total nanostructure surface and ε_a is the evaporation energy, and ψ_{BE} is the surface flux of adatoms from nanowall borders to the two-dimensional vapor on the substrate surface, $\psi_{BE}=\frac{l}{\lambda}\nu_0\exp(-\varepsilon_a^{(2)}/kT)$, where $\varepsilon_a^{(2)}$ is the energy of evaporation to the two-dimensional vapor. The details of relevant surface processes are described elsewhere.[32,33]

The growth dynamics of a nanowall are described by

$$\frac{\partial V_S}{\partial x}da + \frac{\partial V_S}{\partial h}dh = \lambda^3\psi_T dt, \tag{6}$$

where V_S is the volume of an individual nanostructure, and $\frac{\partial V_S}{\partial x}$ and $\frac{\partial V_S}{\partial h}$ are the growth functions that depend on the nanowall size and shape. The main attention here will be paid to the uniformity of the nanowall width distribution. This emphasis is most relevant to advanced stages of nanostructure development, when their height increase is slowed down but they continue widening in the x direction due to continuing delivery of particles from the gas phase and over the surface. This is also very relevant to the CVD/PECVD-based coating of the developed (prefabricated) quasi-two-dimensional structures with functional nanolayers that need to be deposited uniformly over the complex 2D shape. In this case, the nanowall growth functions were assumed in the form $\partial V_S/\partial x=hL_S$, $\partial V_S/\partial h=aL_S/2$, where L_S is the length (in the y' direction) of the nanowall.

In our numerical experiments, the simulation domain was bounded in the x and y directions (substrate surface plane) by the rectangular substrate area 5×5 μm, accommodating 400 nanostructures of our interest here. The average base width of the nanowalls is $a=40$ nm, and the height is $h=300$ nm. It was also assumed that the base widths of the nanowalls are distributed according to the Gaussian law within the limits of 20 − 50 nm. The spacing (in the x direction) between the nanostructures was chosen randomly assuming that no special (e.g., by using lithographic of focused ion beams) surface prepatterning was made. As boundary conditions at the substrate borders, the mean density of absorbed particles on the entire surface was used. At the borders of each individual nanowall, we computed the net surface flux

$$\psi = (\psi_S)_i - (\psi_{SE})_i, \tag{7}$$

where $(\psi_S)_i$ and $(\psi_{SE})_i$ are the surface influx and surface evaporation, respectively. Equation (7) is, in fact, the set of N_n equations, where $N_n=400$ is the total number of nanowalls on the surface. Gas pressure was assumed P=1–5Pa, the initial surface coverage by the nanostructures was assumed $\mu=0.1$.

The set of the plasma, nanostructure, surface, and other process parameters used in this series of numerical experiments is summarized in Table I.

III. NUMERICAL RESULTS

Figure 2(a) shows a representative distribution of the ion current on the lateral surface of a typical nanowall. It is seen that the ion current is effectively redistributed in the electric field created by the nanostructures. Furthermore, the density of the ion current in the upper part of the nanostructure is significantly increased and becomes larger than its mean value on the open surface areas uncovered by nanowalls. A profile of the computed adatom density in the trenches between the quasi-two-dimensional nanostructures is shown in Fig. 2(b) for the surface coverage $\mu=0.12$. The golden strips correspond to the nanostructure bases. It is seen that the surface density peaks in the areas between the nanowalls and tends to the equilibrium density near the nanostructure borders.

A representative three-dimensional picture of the temporal evolution of the nanowall width distribution function in the neutral gas process of 1 Pa pressure is shown in Fig. 3. It is notable that the initial distribution changes with time and also broadens. The maximum of the distribution function decreases with time. We should mention here that in the simulations we did not account for a possible coalescence of nanowalls during their broadening, and limited our consideration by the surface coverage not exceeding 0.5, when the probability of any overlap of the nanostructures is low. Thus, in the range of surface coverages used we managed to avoid any overlap or coalescence of individual growing nanostructures, keeping the number of nanowalls invariable. The final distribution function appears to be significantly wider than the initial one, thus reflecting a larger and continuously increasing dispersion of the nanostructure widths. The quantitative results of these calculations are presented in Fig. 4, which shows the final width distribution function for the plasma-based process in dense plasma at 2 eV, and a similar distribution for the neutral gas process at 5 Pa. The maximum values and widths of the distribution functions differ significantly, with the width distribution function much wider for the neutral gas process.

Thus, our hybrid simulations, which involve the ion motion and adatom surface diffusion submodules, provide the detailed numerical modeling of the growth kinetics of individual nanowalls. For this purpose, the nanowall growth functions were integrated for each individual nanostructure

TABLE I. Parameters and representative values used in computations.

Parameter	Notation	Value
Nanostructure height	h	300–500 nm
Nanostructure width (in the x direction)	a	20–200 nm
Nanostructure length (in the y direction)	L_s	3–5 μm
Initial nanostructure width	a_0	40 nm
Number of nanostructures in the pattern	N_n	400
Electron energy in the low-temperature plasma	T_e	2–5 eV
Plasma density	n_p	$(1\times10^{17})-(3\times10^{18})$ m^{-3}
Neutral gas temperature	T_g	100–500 °C
Neutral gas pressure	p_0	1–5 Pa
Substrate bias	U_S	−20 V
Substrate area	S_S	5×5 μm
Surface temperature	T	400 °C
Range of surface coverage	μ	0.1–0.5
Number of ions in Monte Carlo simulation	N_i	2×10^5
Mass of ionic/atomic building units	m	12 amu
Sheath width	λ_s	$(8\times10^{-4})-(2\times10^{-2})$ cm
Frequency of lattice atom oscillations	ν_0	10^{14} s^{-1}
Lattice constant	λ	5×10^{-10} m
Dielectric constant of the vacuum	ε_0	8.85^{-12} C V^{-1} m^{-1}
Surface diffusion activation energy	ε_d	0.6 eV
Magnitude of electric field	E	$\sim10^7$ V/m

in the entire nanopattern, under the individual conditions and individual diffusion fluxes determined from diffusion equation (3). Figure 5 shows the dispersion area of individual rates of width change for all 400 nanostructures from the nanopattern as a function of their width. It is seen that the dependence of the individual rates of width change on the nanostructure width is weak, however some decrease in the rate with the width increase is noticeable. This result shows that the commonly used mean-field approximation, in which the individual growth rates for individual nanostructures are calculated by using the *mean* density of adatoms on the surface, should be used with extra care since the positions of individual nanostructures strongly affect their rates of width change; that is why we used a more complex but more accurate model, which enabled the calculation of individual adatom fluxes to each nanostructure in the pattern. The influx of particles to each nanostructure depends strongly on the individual environment in the vicinity of the nanostructure and, in fact, varies widely, thus causing a wide dispersion in the rates of width change observable in Fig. 5. The influence of the nanostructures located near the substrate's edges (and hence affected by quite different growth conditions) was not

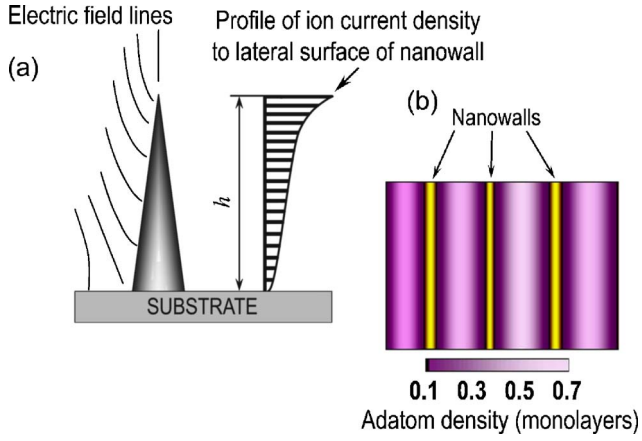

FIG. 2. (Color online) (a) Scheme of electric field lines and representative profile of calculated ion current distribution on the lateral surface of the nanowall; (b) adatom density field on the open surface between nanowalls for surface coverage μ=0.12. Nanowalls (top view) are shown as thin golden strips (not to scale).

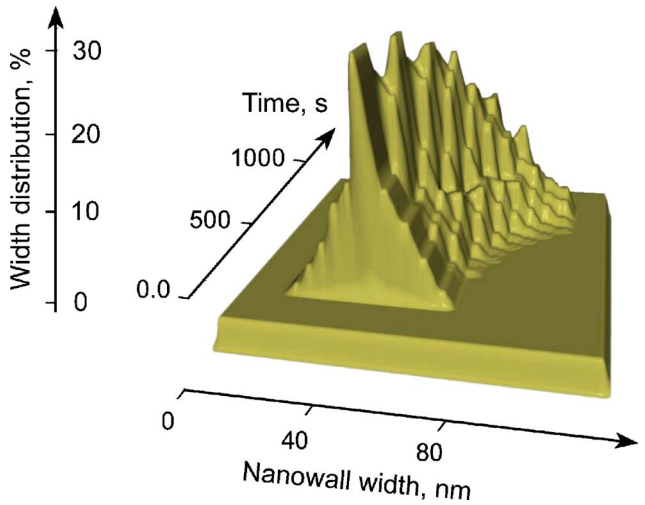

FIG. 3. (Color online) Temporal evolution of nanowall width distribution function in a neutral gas process. The initial distribution broadens with time, thus the final distribution is significantly wider than the initial one.

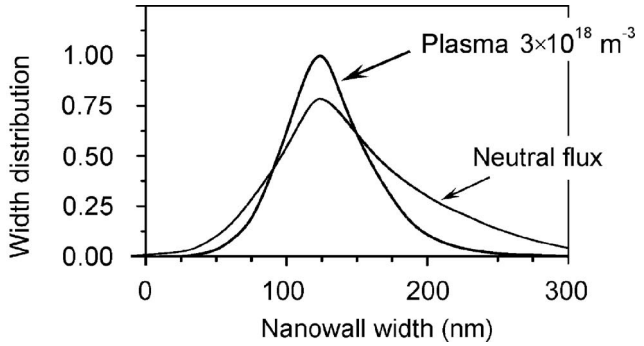

FIG. 4. Distribution function of nanowall width after 1000 s into the growth process for plasma 3×10^{18} m^{-3} and neutral flux.

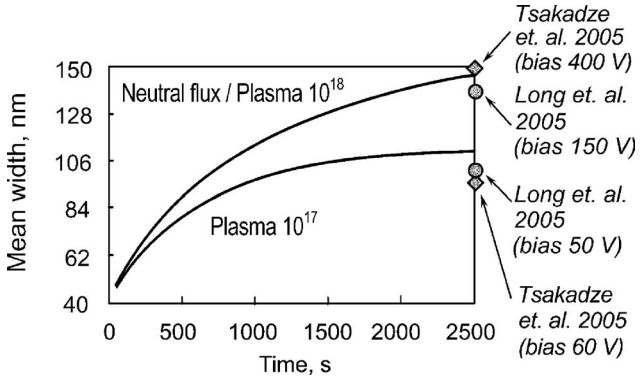

FIG. 6. Dependence of the mean nanowall width on time with plasma density as a parameter, for plasma and neutral processes. Comparison with experimental data is also shown.

accounted for in Fig. 5. We emphasize that in our approach, the growth of *each* nanostructure is simulated individually to work out the statistical characteristics of the entire nanopattern.

Figure 6 illustrates the temporal evolution of the mean width of nanowalls, with the plasma density as a parameter. The nanostructures mean width increases for both the neutral and plasma-based processes. The nanostructures grown from the low-density plasma demonstrate a smaller mean width. Figures 7 and 8 illustrate the dependencies of the square deviation σ of the nanostructures width distribution function on their mean width and deposition time, for plasma of 5 eV and gas pressure of 2 Pa. One can see that the difference in σ is rather strong: at a mean width of 120 nm, the deviation reaches $\sigma=1.9$ in the neutral gas process but remains almost twice as low ($\sigma=1.05$) in the plasma of 3×10^{18} m^{-3}.

IV. DISCUSSION

A. Physical interpretation

It is evident that one of the main advantages of ionized gas-based processes is the increased energy of the incident particles (e.g., ions), as compared with the energies of atoms/molecules in neutral gas. An increased energy of the particle-surface interaction provides a range of beneficial effects, such as heating of the surface, increasing the particles reactivity, control of the surface reactivity via dynamic termination/activation of surface dangling bonds, and several others. As a result, the nanowalls grown by using the plasma may feature an improved structure, crystallinity, and ordering.[34] Besides, the ionized gas processes make it possible to generate reactive species (such as atomic hydrogen) that can cause amorphous to crystalline structural transformations.[35,36] Thus, the use of plasma-based processes for the surface treatment is in most cases more advantageous than the neutral gas-based techniques. Nevertheless, simplicity, convenience, and safety remain the advantages of the gas process, which make it quite difficult to make the final choice of the optimum nanofabrication environment. However, poor "geometrical" controllability in the gas process, which is caused by the diffusion-like, undirected flux of the neutral atoms to the nanostructures, may be a main decisive factor in favor of the plasma-based techniques. Moreover, in neutral gas-based processes, it appears difficult to control the selective delivery of neutral particles to the nanostructures, which in turn compromises the ability to effectively control the main parameters of the nanostructures.

In the plasma process, a better controllability is achieved due to the presence of ionized species in the gas phase and of patterned (focused by the nanostructures) electric field in the immediate vicinity of the nanopattern. This enables one to selectively control the building block delivery processes. In-

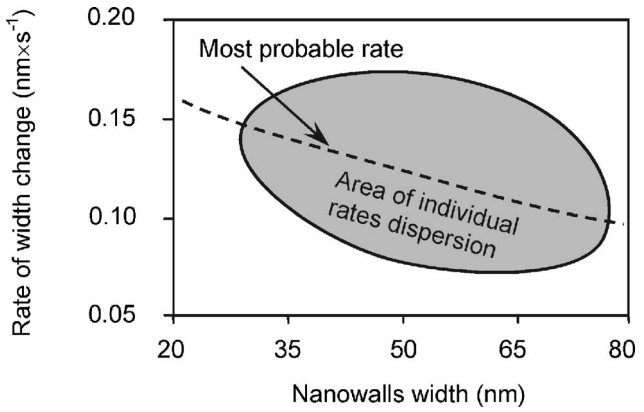

FIG. 5. Dependence of rates of nanowalls width change on their width. A wide dispersion field (shown by gray in the figure) is due to the individual growth conditions of each nanowall.

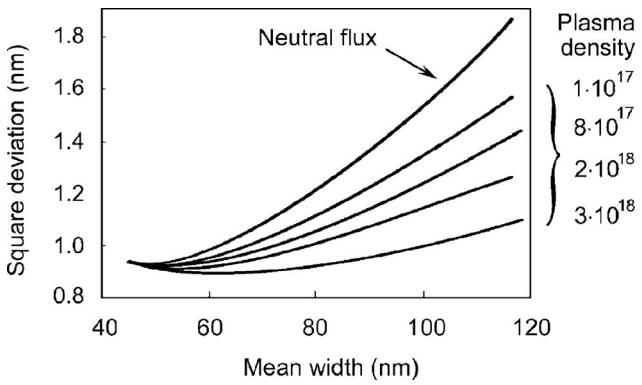

FIG. 7. Dependence of square deviation σ on the mean nanowall width with the plasma density as a parameter.

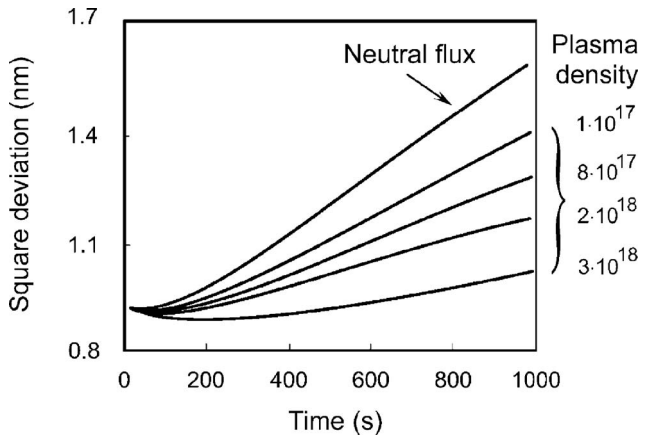

FIG. 8. Dependence of the square deviation on time with the plasma density as a parameter.

deed, it becomes possible to use the microscopic electric field to directly deliver the particles to the lateral surfaces of the nanowalls, which results in a significant increase of the direct (from the gas phase) particle incorporation into the nanostructures as compared with the neutral gas processes. Moreover, the electric field becomes an efficient control in redistribution of the ion flux deposited to different trenches between the nanowalls.

The main distinguishing feature of the nanowalls nanotopology observed in our numerical experiments is the broadening of nanostructure size distributions with time (increasing mean width). To understand this phenomenon, let us examine the diffusion-caused reorganization of the adatom density field on the substrate surface. It is evident that small nanostructures located near larger ones can get into the surface areas with depleted adatom densities. This depletion effectively decreases the diffusion influx to the borders of nanowalls and hence retards their growth. Thus, it turns out that the mutual interaction of growing nanostructures is essential even when the surface coverage is small (0.1 in our case) and should necessarily be taken into account in simulations. This effect has already been illustrated in Fig. 5, where a very wide scattering for the rates of width change of nanostructures is shown. In the neutral gas process, the atom influx to the substrate surface is uncontrollable and the atoms are deposited uniformly on the entire surface. In this case, the above adatom density depletion process strongly affects the growth of smaller nanostructures. On the contrary, narrower nanostructures grown in the plasma create a stronger electric field, which forces the ions to deflect while traversing the sheath and eventually deposit on the substrate surface near the narrower nanowall. Thus, an effective redistribution of the diffusion fluxes takes place, which gives an extra boost for the growth of the narrower nanostructures. As a result of the plasma process, the width distribution function equalizes, and eventually a nanopattern of very similar nanowalls is developed.

Analyzing Figs. 5–8, one can conclude that the plasma process provides a very efficient control of the surface nanotopology. In the dense ($n_p=3.0\times10^{18}$ m^{-3}) plasma-based process, we reported only a small broadening in the width distribution function (Fig. 7), which suggests the possibility of development of size-uniform quasi-two-dimensional nanopatterns. In less dense plasmas, the square deviation increases and reaches 1.5 for $n_p=1.0\times10^{17}$ m^{-3}. However, the gas process shows a square deviation much larger (reaching 1.9) than in the plasma-based processes.

B. Analysis of relevant experimental data

To justify the model implemented and assumptions used, we have made a direct comparison of the results of our numerical simulations with those obtained from the experiments. To demonstrate the key role of the ion current focusing by nanostructures, we have shown the results of the experiment on carbon nanostructure formation at different substrate biases. In Fig. 9, we show SEM photographs of the carbon nanostructures grown on a biased substrate in an inductively coupled plasma (ICP) assisted process. In this experiment, the plasma density and substrate surface were not changed, and the substrate bias was the only variable parameter. A detailed description of the experiment and facility can be found elsewhere.[37] This experiment evidences the importance of the ion current redistribution by the nanostructure-generated electric field. At the low bias close to that used in our numerical simulations, nanostructures were synthesized with a mean width of about 70 nm, which is close to the calculated value 105 nm.

At the high bias conditions, our model predicts a weaker ion current focusing due to the increase of the plasma-surface sheath width, which can be calculated as

$$\lambda_S=\left(\frac{\sqrt{3}}{2}\right)\lambda_D\left(\frac{2U_S}{T}\right)^{3/4},$$

where $\lambda_D=(\varepsilon_0 T_e/n_p e)^{1/2}$ is the Debye length and n_p is the electron density in the plasma. Thus with the bias increasing,

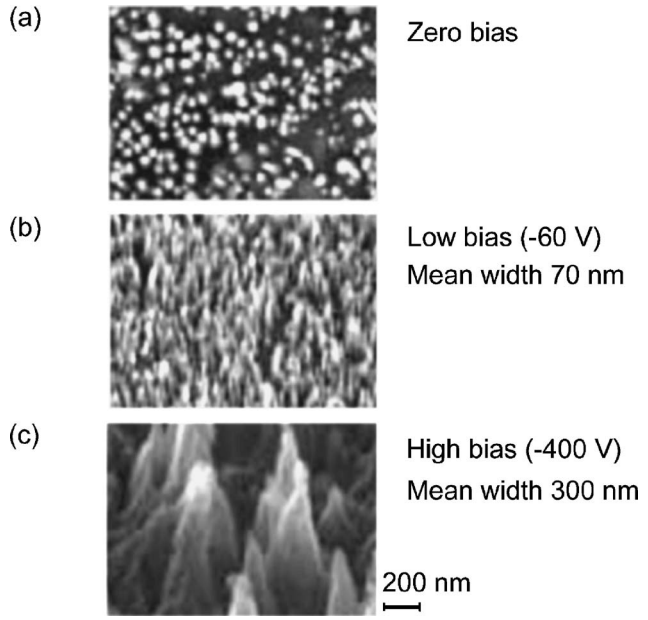

FIG. 9. Carbon nanostructures synthesized in ICP plasma. (a) Zero bias, (b) low bias (60 V), (c) high bias (−400 V). Photo courtesy of Z. L. Tsakadze, S. Xu, and K. Ostrikov (unpublished).

TABLE II. Computed and experimental values of nanostructure width.

Parameter	Value	Ref.
Mean width of nano-	130	Calculated (this work)
structures synthesized in	140	38
high-density plasma/high	150	39
bias conditions, a (nm)	150	Measured (Fig. 9)
Mean width of nano-	105	Calculated (this work)
structures synthesized in a	100	38
low-density plasma/low	80	39
bias conditions, a (nm)	70	Measured (Fig. 9)

the sheath width increases and the influence of the electric field due to the nanostructures on ion motion in the vicinity of nanostructures becomes less noticeable. As a result, the ion current is collected only by the highest nanostructures, which grow predominantly. Eventually, the nanopattern that consists of large nanostructures of small surface density is formed; a representative pattern can be seen in Fig. 9(b). Similar data were reported by Long *et al.*[38] and Tsakadze *et al.*[39] In particular, in the nanostructures formed at a zero bias (without the ion focusing), only nanoparticles of a low height (comparable with the width) were formed.[39] A quantitative comparison of the nanostructure sizes obtained in our calculations and in several experiments is shown in Table II.

The effect of the plasma density on the nanostructure shape has also been studied experimentally[40] and we have compared these experimental results with the results of our computations. Indeed, it was demonstrated in the experiment that both zero-power (no plasma) and high-power (plasma of higher density) conditions cannot provide a dense, uniform nanostructure pattern.[40] When a plasma of a lower (about 2×10^{17} m^{-3}) density was used, a dense pattern was formed with the nanostructure width of about 70 nm, in contrast to the nanostructures of 150–200 nm formed under conditions of a higher plasma density. Similar computational results are presented in Fig. 6, where several experimental points are also shown.

One more assumption made in this work is that the ions incorporate into the growing structure at the point of collision. It was already mentioned in Sec. II that the ion energy (several tens of eV) is sufficient for activation of hydrogen-terminated bonds; hence the conditions for the atom incorporation are met. Direct MD simulations have shown that the carbon atoms with energy in the range from 1 to 150 eV (thus corresponding to the energies used in our simulations) attached carbon surfaces close to the impact point, without any significant penetration; the latter does not exceed one lattice parameter.[41] Also, Hiramatsu *et al.*[42] have shown that the carbon nanowall width saturates when the nanowall height reaches 300–500 nm; this saturation demonstrates that energetic carbon atoms incorporate into the structure close to the place where they land. A linear increase in nanowall height with time was also reported by Shiji.[43] We reiterate that the results of our computations are consistent with the experimental findings.[37–43]

C. Plasma-based processes: Competitive advantage

Thus, we have demonstrated here that the plasma-aided process, in contrast to the neutral flux deposition process, does provide a very efficient control of the surface nanotopology. Moreover, the use of the ion flux in addition to the neutral one ensures a much better uniformity of the nanostructure sizes. We emphasize that we did not aim at investigating any specific means for the size control in the plasma-aided process—this will be a subject of our future investigations. Nonetheless, we have revealed a superior potential of the plasma-based processes to achieve the as yet elusive deterministic shape control of selected nanostructures. The results of this work enable us to state that in the plasma-based process, one can control the surface nanoscale morphology in the range from $\sigma=1$ to 2 by changing, for example, the plasma density and degree of ionization. Physically, this control has been achieved by varying relative intensities of the direct (from the gas phase) and diffusion (over the surface) fluxes to the nanostructure surfaces, which is impossible in the neutral gas. Besides, it is worth mentioning that the structure and geometrical shape of the nanowalls also depend on the ratio of direct/diffusion fluxes. An increased influx of the particles directly to the nanostructures and their redistribution about their lateral surface will lead to notable changes in the surface nanoscale morphology. This was convincingly demonstrated in experiments on synthesizing carbon nanostructures from a plasma at low (80 V) bias and different surface temperatures.[25] In this case, with the same substrate bias and plasma density, the distribution of direct from the plasma and diffusion fluxes to the growing nanostructures was the main physical parameter changed. The experiments suggest that the use of lower substrate temperatures, when the surface diffusion becomes negligible and the growth is mainly provided by the direct influx from the plasma, leads to the formation of regular and clearly resolved nanostructures.

D. Comments on the assumptions made

Therefore, the available experimental results support the model used in our computations. We used a simplified model that did not include a number of secondary surface and plasma phenomena. The main accent was made on the processes of delivery of charged ions by using nonuniform electric fields in the plasma sheath, and delivery of neutral particles via the surface diffusion of adatoms. The use of two growth functions [Eqs. (6)] in our model presumes that we consider here the nanostructures width increase by atom attachment to the borders of the sp2-bonded carbon sheets [which are usually directed in parallel to the substrate, see Ref. 37 for the experimental results and *ab initio* Density Functional Theory (DFT) calculations], and the nanostructures height increase by formation of new carbon sheets. We did not consider the adatom nucleation on the surface resulting in the origin of new islands in the trenches between the nanostructures. This assumption is valid in the case of reasonably large nanostructures (with the mean width exceeding 40 nm), when the presence of small nuclei of the subnanometer size becomes unimportant. Thus, our simple yet compre-

hensive and experimentally justified model covers all the major processes and enabled us to demonstrate that the plasma process provides a better controllability of the nanowalls nanopattern formation as compared to the neutral gas process.

V. SUMMARY

In conclusion, we have reported the comparative results of numerical simulation of the development of surface nanotopology in neutral and ionized gas-based processes. We have demonstrated that only the slightest broadening in the nanostructures width distribution takes place when a dense plasma is used. The square deviation of the nanostructures widths increases to 50% in less dense plasmas, and reaches 90% in the neutral gas process. We have shown that the plasma-aided process influences strongly, due to the direct delivery of the particles to the growing structures, the width of nanostructures, thus demonstrating an outstanding promise of the plasma nanofabrication process to achieve the as yet elusive deterministic control of nanostructure growth processes and, ultimately, their physical characteristics and functionalities that are so necessary for the development of the next-generation nanodevices.[44–46] The results of our computations are consistent with the presently available experimental results.

ACKNOWLEDGMENTS

This work was supported by the Australian Research Council, the University of Sydney, and the International Research Network for Deterministic Plasma-Aided Nanofabrication.

[1] M. Law, D. J. Sirbuly, J. C. Johnson, J. Goldberger, R. J. Saykally, and P. Yang, Science **305**, 1269 (2004).
[2] Z. Wang, L. L. Daemen, Y. Zhao, C. S. Zha, R. T. Downs, X. Wang, Z. L. Wang, and R. J. Hemley, Nat. Mater. **4**, 922 (2005).
[3] Y. Wu, P. Qiao, T. Chong, and Z. Shen, Adv. Mater. (Weinheim, Ger.) **14**, 64 (2002).
[4] M. Hiramatsu, K. Shiji, H. Amano, and M. Hori, Appl. Phys. Lett. **84**, 4708 (2004).
[5] Y. C. Hong, J. H. Kim, C. U. Bang, and H. S. Uhm, Phys. Plasmas **12**, 114501 (2005).
[6] H. Huang, O. K. Tan, Y. C. Lee, M. S. Tse, J. Guo, and T. White, Nanotechnology **17**, 3668 (2006).
[7] Y. Zhang, X. Song, J. Zheng, H. Liu, X. Li, and L. You, Nanotechnology **17**, 1916 (2006).
[8] J. C. Johnson, H. Q. Yan, R. D. Schaller, L. H. Haber, R. J. Saykally, and P. D. Yang, J. Phys. Chem. B **105**, 11387 (2001).
[9] S. Wang, G. J. Yu, J. L. Gong, Q. T. Li, H. J. Xu, D. Z. Zhu, and Z. Y. Zhu, Nanotechnology **17**, 1594 (2006).
[10] P. P. Rutkevych, K. Ostrikov, S. Xu, and S. V. Vladimirov, J. Appl. Phys. **96**, 4421 (2004).
[11] K. Ostrikov, Rev. Mod. Phys. **77**, 489 (2005).
[12] K. Ostrikov, S. Vladimirov, M. Y. Yu, and G. E. Morfill, Phys. Plasmas **7**, 461 (2000).
[13] K. B. K. Teo, D. B. Hash, R. G. Lacerda, N. L. Rupesinghe, M. S. Bell, S. H. Dalal, D. Bose, T. R. Govindan, B. A. Cruden, M. Chhowalla, G. A. J. Amaratunga, M. Meyyappan, and W. I. Milne, Nano Lett. **4**, 921 (2004).
[14] P. P. Rutkevych, K. Ostrikov, and S. Xu, Phys. Plasmas **14**, 043502 (2007).
[15] K. Ostrikov, Phys. Plasmas **12**, 062105 (2005).
[16] S. V. Vladimirov and K. Ostrikov, Phys. Rep. **393**, 175 (2004).
[17] I. I. Beilis and M. Keidar, Phys. Plasmas **5**, 1545 (1998).
[18] P. P. Rutkevych, K. Ostrikov, and S. Xu, Phys. Plasmas **12**, 103507 (2005); **14**, 043502 (2007).
[19] M. Keidar, I. D. Boyd, and I. I. Beilis, Phys. Plasmas **8**, 5315 (2001).
[20] M. Keidar and I. I. Beilis, Phys. Plasmas **13**, 114503 (2006).
[21] M. Keidar and A. M. Waas, Nanotechnology **15**, 1571 (2004).
[22] S. V. Vladimirov and N. F. Cramer, Phys. Rev. E **62**, 2754 (2000).
[23] I. Denysenko, J. Berndt, E. Kovacevic, I. Stefanovic, V. Selenin, and J. Winter, Phys. Plasmas **13**, 073507 (2006).
[24] I. Denysenko, M. Y. Yu, and N. A. Azarenkov, Phys. Plasmas **13**, 013505 (2006).
[25] Z. L. Tsakadze, K. Ostrikov, J. D. Long, and S. Xu, Diamond Relat. Mater. **13**, 1923 (2004).
[26] S. Xu, K. Ostrikov, J. D. Long, and H. Y. Huang, Vacuum **80**, 621 (2006).
[27] I. Denysenko, M. Y. Yu, L. Stenflo, and N. A. Azarenkov, Phys. Plasmas **12**, 042102 (2005).
[28] E. Tam, I. Levchenko, and K. Ostrikov, Phys. Plasmas **14**, 033503 (2007).
[29] I. Levchenko and K. Ostrikov, J. Phys. D **40**, 2308 (2007).
[30] I. Levchenko and O. Baranov, Vacuum **72**, 205 (2003).
[31] I. Levchenko, K. Ostrikov, and E. Tam, Appl. Phys. Lett. **89**, 223108 (2006).
[32] A. E. Rider, I. Levchenko, and K. J. Ostrikov, J. Appl. Phys. **101**, 044306 (2007).
[33] I. Levchenko, A. E. Rider, and K. Ostrikov, Appl. Phys. Lett. **90**, 193110 (2007).
[34] C. S. Lee, B. Khang, and A. L. Barabási, Appl. Phys. Lett. **78**, 984 (2001).
[35] V. Ligatchev, Physica B **337**, 333 (2003).
[36] S. Sriraman, S. Agarwal, E. S. Aydil, and D. Maroudas, Nature **418**, 62 (2002).
[37] K. Ostrikov, J. D. Long, P. P. Rutkevych, and S. Xu, Vacuum **80**, 1126 (2006).
[38] J. D. Long, S. Xu, S. Y. Huang, P. P. Rutkevych, M. Xu, and C. H. Diong, IEEE Trans. Plasma Sci. **33**, 240 (2005).
[39] Z. L. Tsakadze, K. Ostrikov, and S. Xu, Surf. Coat. Technol. **191**, 49 (2005).
[40] K. Shiji, M. Hiramatsu, A. Enomoto, M. Nakamura, H. Amano, and M. Hori, Diamond Relat. Mater. **14**, 831 (2005).
[41] E. B. Halac, M. Reinoso, A. G. Dall'Asén, and E. Burgos, Phys. Rev. B **71**, 115431 (2005).
[42] M. Hiramatsu, K. Shiji, H. Amano, and M. Hori, Appl. Phys. Lett. **84**, 4708 (2004).
[43] K. Shiji, M. Hiramatsu, A. Enomoto, M. Nakamura, H. Amano, and M. Hori, Diamond Relat. Mater. **14**, 831 (2005).
[44] K. Ostrikov and A. B. Murphy, J. Appl. Phys., J. Phys. D **40**, 2223 (2007).
[45] K. Ostrikov, IEEE Trans. Plasma Sci. **35**, 127 (2007).
[46] Q. Cheng, S. Xu, J. Long, and K. Ostrikov, Appl. Phys. Lett. **90**, 173112 (2007).